Preliminary Design of a Truss-Braced Natural-Laminar-Flow Composite Wing via Aeroelastic Tailoring

(Received: March 04, 2015. Revised: July 15, 2015. Accepted: Sept. 24, 2015)

GUANGQIU WANG[1]
JIE ZENG[2]
JEN-DER LEE[3]
XI DU[4]
XIAOWEN SHAN[5]

Abstract
This paper describes a conceptual feasibility study of a high aspect ratio truss-braced wing configuration. It is known that increased aspect ratios, thinner wings and less sweep angle enable significant drag reduction through natural-laminar-flow. However, it may lead to increased wing weight to avoid aeroelastic issues. Current aspect ratios of conventional aircraft are limited by the structural weight and wing stiffness. To validate the truss-braced high aspect ratio wing concept, the aerodynamics, structural, and weight distribution of a truss-braced natural-laminar-flow composite wing model is firstly created, and the ASTROS (Automated STRuctural Optimization System) software is applied for aeroelastic tailoring optimization. The objective of the study is to minimize the aircraft wing weight, subject to multiple constraints such as structural strength and aeroelastic constraints. The results of this study show that the truss-braced natural-laminar-flow composite wing with high aspect ratio can reduce the fuel consumption significantly compared to the conventional commercial aircraft configuration, and has the great potential in the future commercial aviation market.

1 Introduction

It is well known that high aspect ratio wings can reduce the induced drag effectively[1]. However, the bending moment of the wing roots of the high aspect ratio wings is drastically larger than that of the conventional wings. From structural design point of view, if no additional structures are applied to support the wing, it is not feasible to design such high aspect ratio wings without paying huge weight penalty. The strut/truss braced wing has already been successfully implemented both in the early days of aviation and today's small airplanes. For example, two different truss-braced wing configurations are illustrated in Figure 1(a) and Figure 1(b), respectively.

In the early days of aviation, the external structure has been adopted to support the thin airfoil section to sustain the aerodynamic loads. However, these external structures caused significant drag penalty. It was then gradually realized that if an appropriate structural wing box and suitable thickness-to-chord ratios were adopted, the cantilever wing could be used to replace the strut/truss braced wing. Therefore, lower drag can be achieved.

Even though the cantilever wing configuration has already demonstrated its excellent aerodynamic performance, the concept of the strut/truss braced wing configuration still survived. Compared to the cantilever wing configuration, the increased span of the strut/truss braced wing reduces induced drag, and the decreased wing thickness can reduce transonic wave drag. Hence, a reduced sweep angle can be allowed to improve the aerodynamic performance of the aircraft remarkably [2, 3].

The idea of using strut-braced wing for a long range, transonic transport airplane was first proposed by Werner Pfenninger in the early 1950s [4]. Following Pfenninger's

[1] Vice President, Beijing Aeronautical Science & Technology Research Institute of COMAC,102211, Beijing, Chinawangguangqiu@comac.cc
[2] Technical Fellow, Beijing Aeronautical Science & Technology Research Institute of COMAC,102211, Beijing, zengjie@comac.cc
[3] Technical Fellow, Beijing Aeronautical Science & Technology Research Institute of COMAC,102211, Beijing,lizhengde@comac.cc
[4] Senior Aerospace Engineer, Beijing Aeronautical Science & Technology Research Institute of COMAC,102211, Beijing, duxi@comac.cc
[5] Technical Fellow, Beijing Aeronautical Science & Technology Research Institute of COMAC,102211, Beijing, shanxiaowen@comac.cc

doi:10.3293/asdj.2015.36

a) Cessna 172

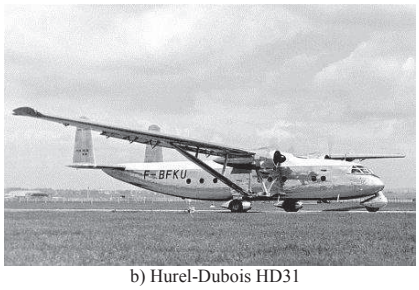

b) Hurel-Dubois HD31

Figure 1: Strut/truss-braced wing configuration.

Figure 2: The concept of the strut-braced wing. red: surface with turbulence effect, blue: surface with natural laminar flow effect.

work, other strut-braced wing researches have also been performed to evaluate the aerodynamic performance of this concept [5, 6, 7]. However, none of this research was performed using multidisciplinary design optimization (MDO). However, because of the tight coupling between the aerodynamics and structures during the strut-braced wing design process, an MDO approach is required to evaluate the concept.

Due to its great potential of drag reduction, NASA started to financially support the research on strut-braced wing concept using MDO approaches. Since then, much research has been performed on the strut-braced wing and truss-braced wing using MDO approaches [8, 9, 10, 11, 12, 13, 14, 15, 16, 17, 18]. All of these results demonstrated the feasibility of adopting the strut-braced wing or truss-braced wing.

Nowadays, due to the soaring of the fuel price and the environmental concerns, special attention is being paid to the aircraft with lower fuel consumption and low emissions [19, 20]. According to this, NASA defined the future scenario, concepts and technology for future commercial transport airplanes. From NASA's concept, Boeing737 Next generation (737-600/-700/-800/-900ER) and CFM56 engine are served as the standard, and are defined as 'N+1', i.e., the baseline configuration. The advanced configuration defined as 'N+3', will be served after 2040. Among these 'N+3' design configurations, the high aspect ratio natural-laminar-flow wing configuration has been considered as the one that has the most splendid future. According to this, NASA issued the Subsonic Ultra Green Aircraft Research (SUGAR) program in 2010, to support Boeing in performing the feasibility study of the strut-braced wing configuration [21, 22].

In Boeing's SUGAR program, detailed performances of both the reference conventional aircraft configuration and the advanced unconventional aircraft configuration were thoroughly studied and compared, which included fuel burn, emissions, noise, take off performance, etc. Finally, the technology development roadmaps for the future green aircraft were generated. The basic concept for the strut-braced wing built in Boeing's SUGAR program is illustrated in Figure 2.

In this paper, a truss-braced wing aircraft model similar to a truss-braced wing, named 765-095-TS1 N+4 in [22] is studied. In addition, both conventional metal material and advanced composite material are considered for the wing structure design. Since the advanced composite material has superior specific stiffness and strength characteristics, it can be designed to meet the directional stiffness/strength requirement through aeroelastic tailoring optimization [23, 24]. Therefore, the goal of the research is to apply aeroelastic tailoring technique for a preliminary design of a subsonic, truss-braced natural-laminar-flow composite wing, thereby validating the feasibility of the concept. To perform a high fidelity analysis for this conceptual design study, the aerodynamics, structural, and weight distribution of a truss-braced natural-laminar-flow

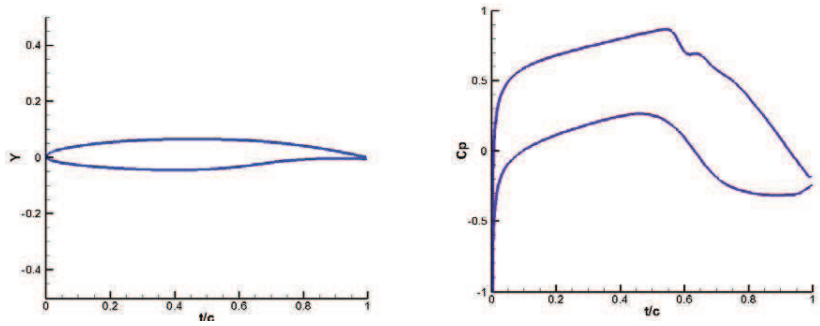

(a) Designed Airfoil shape

(b) Representative Pressure Distribution at 70% Semi-Span (Computed at M 0.74, α 0.4, Re 14.6880)

Figure 3: Natural laminar flow airfoil.

composite wing model is firstly explored, and then several aeroelastic design and analysis tools such as ZEUS (ZONA Euler Unsteady Solver), ZAERO and ASTROS (Automated STRuctural Optimization System) are applied and integrated for the optimization purposes.

2 Problem Statement

The purpose of this research is to design a composite wing structure and investigate the potential of the truss-braced natural-laminar-flow wing with high aspect ratio. The aerodynamic shape of a truss-braced wing is designed based on the following considerations:

1. Due to the flexibility of the high aspect ratio wing, the truss-braced wing is applied.
2. To avoid the wake of the truss and wing, the engine is placed under the wing.
3. To avoid the effect of the wake of the wing to horizontal tail, a T-tail is adopted.
4. The airfoil is a natural-laminar-flow airfoil designed with inverse design approach by providing the target pressure distribution. An adjoint approach is used to compute the gradient required for gradient-based optimization and an automatic laminar-turbulent transition prediction module is also included. The airfoil features 50% of natural laminar flow on upper surface at the designed Mach number and lift coefficient. Figure 3 shows the airfoil shape at 70% semi-span with a representative pressure distribution.
5. The parameters of aerodynamic model refers to Boeing's SUGAR program [21], such as aspect ratio, taper ratio, dihedral, and sweep angle.
6. The position of truss refers to that which is specified in SUGAR program [22].
7. The dimension of the horizontal tail and T-tail is similar to that of B737.
8. The folding position of the wing refers to that which is specified in SUGAR program [22].

The main aerodynamic shape parameters of such truss-braced wing aircraft is given in Table 1. The 3D view is shown in Figure 4.

The optimization task for the truss-braced composite wing structure design in ASTROS [25] can be defined in a mathematical form as:

Find the set of design variables, ν, that can minimize an objective function:

$$F(\nu) \tag{1}$$

subject to constraints:

$$g_j(\nu) \leq 0.0, \qquad j = 1, \ldots, ncon \tag{2}$$

Table 1: The main parameters of a truss-braced wing aircraft.

	Wing	Horizontal Tail	Vertical-Tail
Area(mm^2)	1.2494e8	2.1862e7	2.2115e7
Aspect Ratio	23.097	1.522	4.388
Taper Ratio	0.173	0.366	0.370
Dihedral($^\circ$)	0.0	-	-6.0
1/4 chord sweep($^\circ$)	5.0	35.24	29.60
root chord(mm)	3813.5	5550.4	3277.5
tip chord(mm)	661.4	2029.0	1212.4
span (mm)	52720.0	-	9851.2

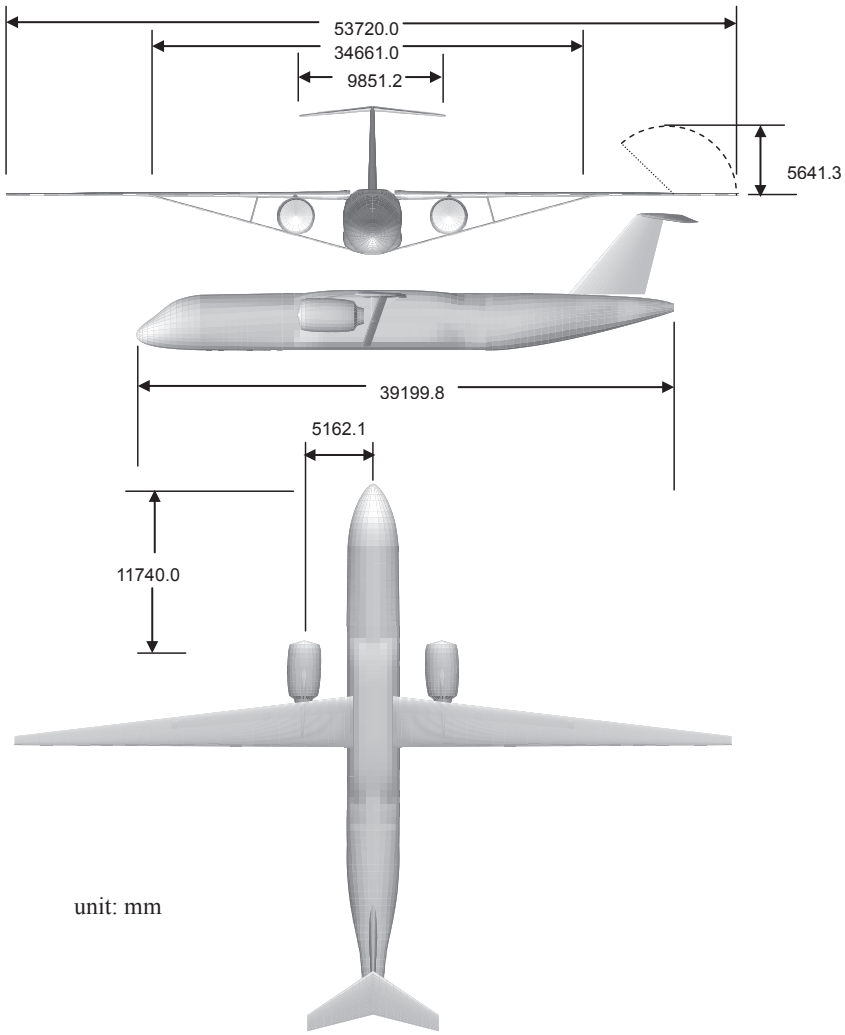

Figure 4: The 3-D view of a truss-braced wing aircraft.

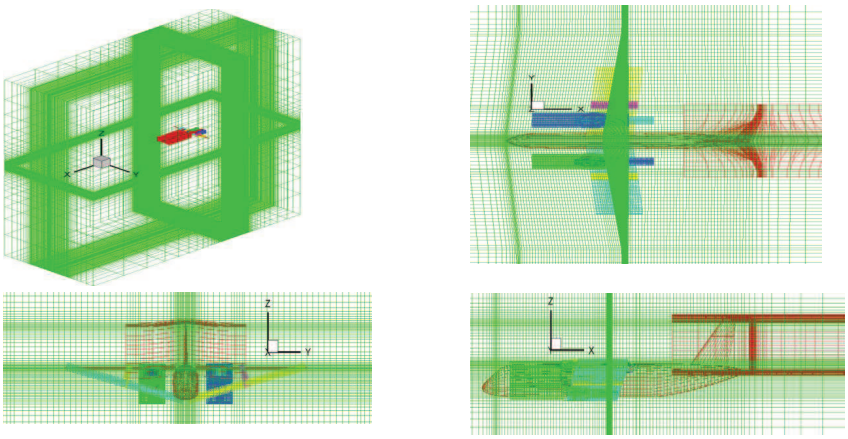

Figure 5: The overset mesh generation of truss-braced wing aircraft using ZEUS.

$$h_k(\nu) = 0.0, \qquad k = 1, \ldots, ne \tag{3}$$

$$\nu_i^{lower} \leq \nu_i \leq \nu_i^{upper}, \qquad i = 1, \ldots, ndv \tag{4}$$

where g specifies the $ncon$ inequality constraints and h refers to the ne equality constraints. Equation 4 specifies lower and upper bounds (side constraints) on each of the design variables

In this research, the objective function $F(\nu)$ is chosen as the weight of the truss-braced composite wing structure, subject to the required flutter speeds, without exceeding allowable strain constraints. In addition, the design variables are the thickness of each composite layer on those elements for modeling the wing and truss skins and the thickness of the aluminum spars and ribs.

3 Aerodynamic Model

The aerodynamic models of the truss-braced natural-laminar-flow composite wing aircraft are created using ZAERO [26], and ZEUS [27], separately.

In this research, ZEUS(ZONA Euler Unsteady Solver) is used to compute three different set of data:

1. Lift coefficient and drag coefficient at different Mach numbers, to determine the best cruise Mach number and altitude.

2. Steady flow computation from Mach 0.6 to 0.785, to be used as the steady flow input for the ZTRAN method in ZAERO software.

3. Steady aeroelastic analysis at 2.5g pull up, -1.0g push-over, and $\pm 25^\circ$ aileron deflection to generate critical design loads.

ZEUS solves Euler equations with boundary layer coupling option. The overset mesh capability in ZEUS is used to handle complex configuration such as the truss-braced wing aircraft in this study. Figure 5 illustrates an overset mesh of the truss-braced wing aircraft used in this paper. From Figure 5, ten blocks are used in total: block 1 for wing and body, block 2 for T-tail, block3/4 for left/right engine, block 5/6 for left/right pylon, block 7/8 for left/right strut under the wing, and block 9/10 for left/right middle strut under the wing.

It is well known that the transition point from natural laminar flow to turbulent flow has significant effects on the surface friction drag. Even though the advanced CFD techniques have been applied, the transition point still cannot be precisely predicted. For a traditional airfoil, the transition points usually located at 10-20% of the chord length. In this study, a natural laminar flow airfoil was specially designed to improve the percentage of the laminar flow area on the wing. To simplify the study, it is assumed that the transition points are in the range of $[30\% \sim 50\%]$ of the chord length.

Table 2: The cruise mach and altitude at different transition points.

	Trans. Point (30%)	Trans. point (50%)	Boeing SUGAR
Cruise Mach	0.720	0.710	0.730
Cruise Altitude(m)	10300	9600	13400
C_L	0.7457	0.6685	0.775
C_D	0.0333	0.0240	0.02962
C_L/C_D	22.390	28.714	26.163
Mach$\times C_L/C_D$	16.12	20.387	19.09

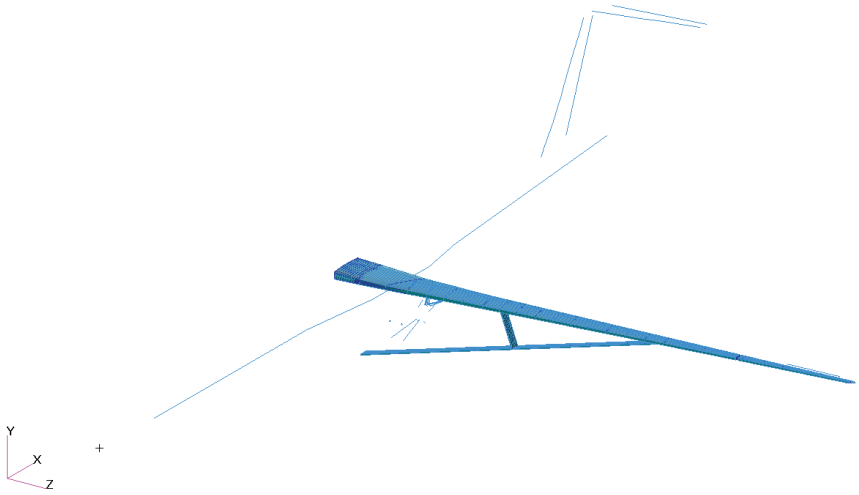

Figure 6: The half NASTRAN structural model.

According to the assumption described above, the cruise Mach and altitude at two different transition points are calculated and summarized in Table 2. In addition, the results obtained from Boeing SUGAR program [22] are also presented in this table for comparison purposes.

4 Structural Model

A baseline structural model of the truss-braced wing aircraft is created for the aeroelastic tailoring study, and is shown in Figure 6. Assuming the structural model is symmetric, only a half span model is required. The symmetric and anti-symmetric natural modes can be obtained by placing symmetric and anti-symmetric boundary conditions at the symmetric plane, respectively.

It should be noted that the structure shown in Figure 6 is the initial design, and will be the input for the following aeroelastic design optimization process.

4.1 Aircraft Fuselage Structural Model

The fuselage structural model consists of beam elements. The bending stiffness EI, torsional stiffness GJ and mass distribution are referred from other same class of commercial aircraft [28]. Figure 7 illustrates the fuselage stiffness data.

4.2 T-Tail and Horizontal Tail Structural Model

The T-tail structural models also consist of beam elements. The bending stiffness EI, torsional stiffness GJ and mass distribution are comparable with other same class of commercial aircraft with T-tail [29]. The joint stiffness of the rudder and elevator are also obtained from the same class of commercial aircraft [29]. Figure 8(a) and (b) present the stiffness of the vertical tail model and horizontal tail model, respectively.

4.3 Pylon and Engine Model

The GENEL element in ASTROS is used to simulate the pylon stiffness. Figure 9(a) shows the detailed pylon model before it is simplified by the GENEL element, and

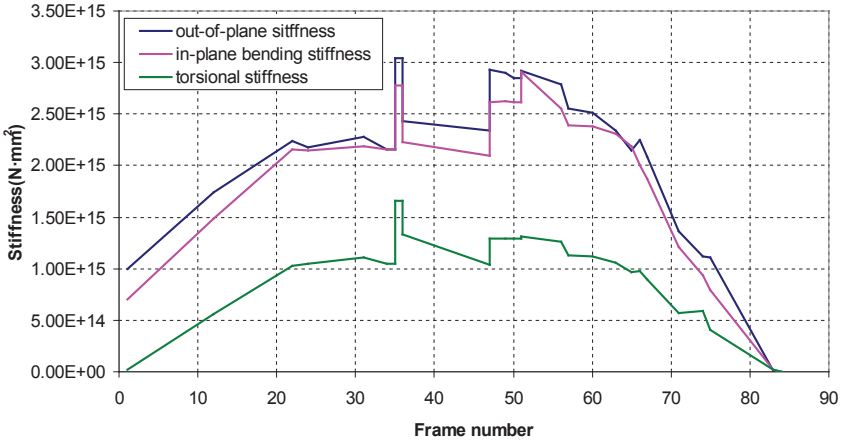

Figure 7: Stiffness of the aircraft body model.

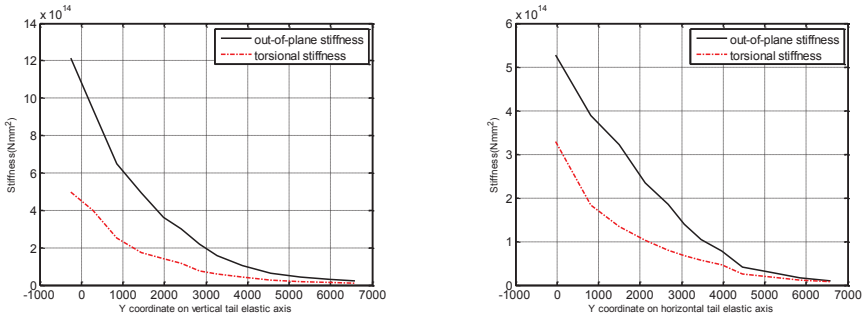

a) Stiffness of the Vertical Tail Model

b) Stiffness of the Horizontal Tail Model

Figure 8: Stiffness of the T-tail model and horizontal tail model.

Figure 9(b) presents the pylon model after it is simplified by the GENEL element. With the GENEL element, only the pylon in-station section, wing connection, bottom wing connection, cross-bar and push-rod are kept, and stiffness of other part is simulated using one GENEL element. In the model simplification process, the same stiffness at the reserved nodes is ensured, and the local modes are neglected. The engine is assumed as a rigid body, and its mass is obtained from CFM LEAP-X engine.

4.4 Wing Structural Model

Wing box is made up of spars, ribs and skins. The spars and ribs are made from aluminum alloy, and the skin is from composite material with four composite laminate $(0°/+45°/-45°/90°)$ layup.layup. The material properties of the aluminum alloy and composite material are given in Table 3.

The wing box ASTROS model consists of front spar, rear spar, and 26 ribs. The front spar and rear spar are broken into two parts at the wing folding position. Two joints are used to connect them. The single torsional stiffness is 2259.7E6 (N·mm), and this joint stiffness is referring to the data of other folding wing aircraft, such as F/A-18

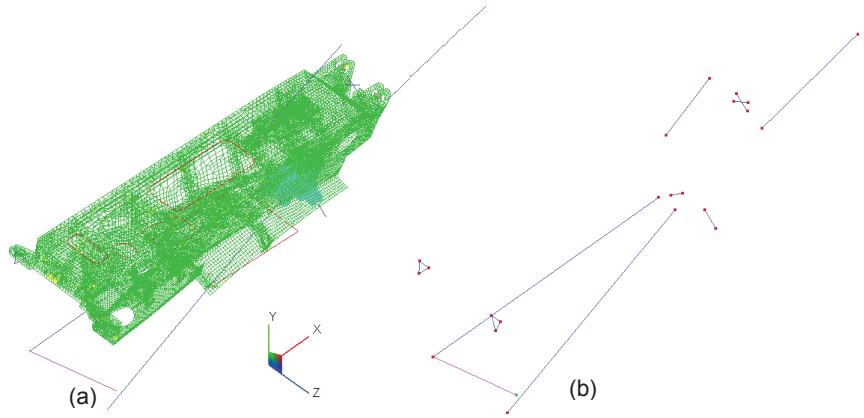

Figure 9: Pylon FEM model before/after simplification.

Table 3: The material properties of aluminum alloy and composite material.

	Young's modulus E(GPa)	Poisson's ratio ν	Limit stain μ strain
aluminum	71.0391	0.3	$\pm$4500
composite	162.0	0.34	$\pm$4500

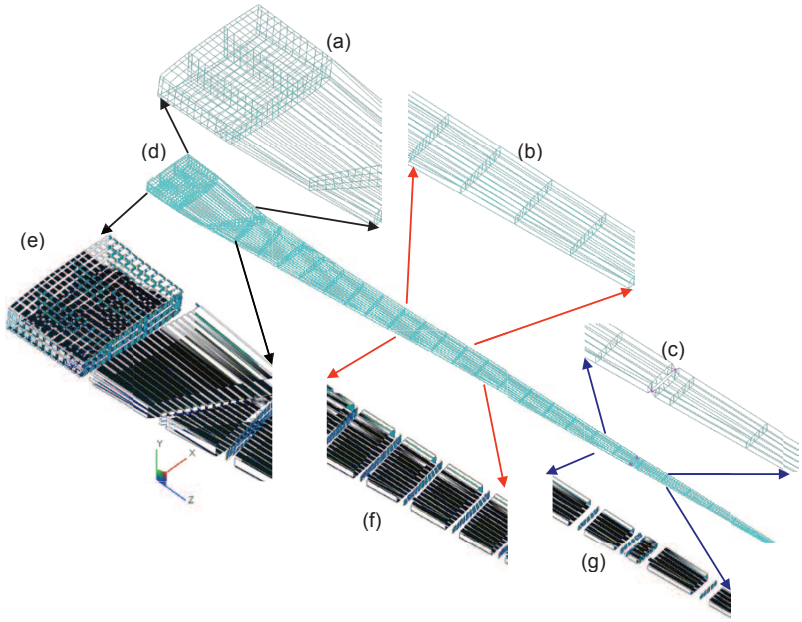

Figure 10: Wing structural model.

[30]. In each side of the wing, the number of elements of spar is 78, the number of elements of rib is 325, and the number of elements of skin is 529. Figure 10 shows the ASTROS structural finite element (FE) model of the wing box. Figure 10 (a)-(c) present the zoom-in view of the wing root, wing section, and wing folding structure. Figure 10(d) is the structural model of the wing box of the whole wing. Figure 10(e)-(g) are the shrunk elements of each part, respectively.

4.5 Truss Model

The truss is also made up of spars, ribs, and skins. The spars and ribs consist of aluminum alloy, and the skin consists of composite material with four composite laminate $(0°/+45°/-45°/90°)$ layup. Figure 11 presents the FEM model of the truss and the wing.

4.6 Payloads, Fuel and Structural Weight

Referring to a similar class commercial aircraft [31], it is assumed that the payloads are 21.30 tons, fuel is 19.56 tons, and structural weight excluding the wing and truss is 35.14 tons. The distribution of the total weight is created using CONM2 card in ASTROS. The distribution of the payload, fuel and structural weight is illustrated in Figure 12.

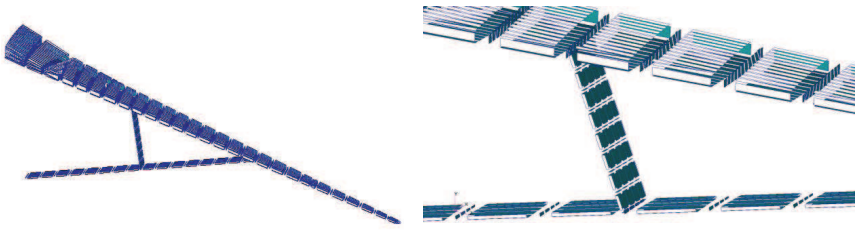

a) FEM Model of Truss and Wing. b) Zoom in Plot.

Figure 11: The FEM model of truss and wing.

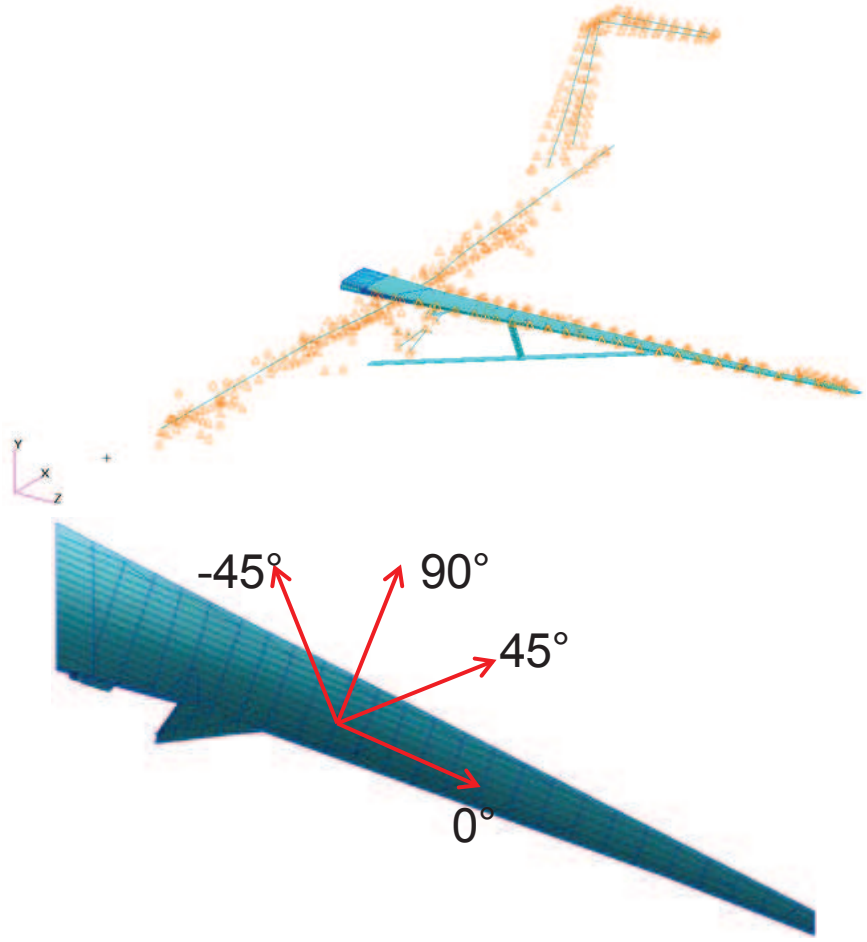

Figure 12: The distribution of payloads, fuel and structural weight.

Figure 13: The orientation of the laminate lay-up.

5 Optimization Strategy

From the description of the previous section, two kinds of materials are used during the design optimization process: aluminum alloy and composite material. Aluminum alloy is used to build spar and rib. The wing and truss skins are constructed using four layers of composite material, which is laminated with $(0°/+45°/-45°/90°)$ orientation, see Figure 13.

5.1 Constraints

To simplify the optimization, only two kinds of critical constraints are implemented during the optimization process.

- Flutter constraint: in the Mach range of $[0.6 \sim 0.8]$, the flutter speed has 15% of margin above the flight envelope..
- Strength constraint: for aluminum alloy, the strain constraint is ± 0.004; for composite material, the strain constraint is $[-0.004 \sim 0.006]$.

5.2 Critical Design Loads

Based on the maximum payloads and maximum fuel condition, four flight maneuvering are selected to compute the critical loads at cruise Mach number 0.72:

1. 2.5g pull-up: This loading condition will induce critical wing-root bending moment and shear.
2. -1.0g push-over: This loading condition will induce critical compressive forces in the wing strut.

3. $\pm 25^{\circ}$ aileron deflection: This loading condition will induce the maximum wing-root torque.

After that, the final critical loads are calculated by multiplying the resulting loads with a design safety factor of 1.5 for wing structural design optimization. Other design loads, such as landing impact loads, gust loads, and maneuver loads are not considered in this research.

5.3 Design Variables

The elements for modeling the fuselage, T-tail, and engine pylon are kept unchanged during the optimization and are retained at their baseline values. All elements for modeling the spars, ribs, and skins of the wing and truss are defined as the design variables. The numbers of plate elements on the wing and truss composite skins are 529 and 200, respectively, and each plate element has four composite layers, leading to 2916 design variables. The number of plate elements for modeling the aluminum spars and ribs of the wing and truss is 100 which correspond to 100 design variables. Therefore, the total design variables are 3016.

5.4 Optimization Framework

The ZONA TRANsonic (ZTRAN) method [32] in ZAERO is employed to generate the Aerodynamic Influence Coefficient (AIC) matrices in the Mach range of $[0.6 \sim 0.8]$. The ZTRAN method requires the steady background flow computed by other CFD code such as ZEUS as input. These AIC matrices are imported into ASTROS to evaluate the flutter constraints at transonic Mach numbers. The critical loads generated as explained in previous section are based on an initial structural design. These critical loads are used by ASTROS sizing optimization to create a new structural design. Therefore, it is imperative to re-calculate the critical loads on this new structural design. Hence, an outer loop iterative process is needed, wherein, the optimization will be iteratively carried out until the structural design variation is negligible. The convergence criterion for such an outer loop iterative process can be defined by the following equation:

$$f = \sum_{j=1}^{l} \sum_{k=1}^{m} (t_{ij}^{n} - t_{ij}^{n-1})^2 \tag{5}$$

where l =total number of skin elements, m = total number of layers in each element, t_{ij} = skin layer thickness in the ith layer and jth element and n = iteration index. The outer loop converges when the result of Equation 5 is very small.

Another technical issue is that the ASTROS sizing optimization may result a non-smooth thickness distribution of each composite layer. This non-smooth thickness distribution may increase manufacturing cost and could create local stress concentration problem. To circumvent this problem, a computer code called SMOOTH was developed that fits the thickness distribution of each layer into a set of Legendre polynomials by a least square procedure. Because each Legendre polynomial is a smooth function, the resulting thickness distribution also will be a smooth function. However, the structural model after applying SMOOTH may not satisfy all the flutter and strength constraints due to the small deviation of the thickness distribution from that of the outer loop design. Therefore, to satisfy those constraints, it is required to perform one more ASTROS sizing optimization referred to herein as the final ASTROS optimization. But this time, the thickness distribution generated by SMOOTH is defined as the lower bound of each design variable so that the optimizer only adds weight to the structure. In so doing, the thickness distribution computed by the final ASTROS optimization does not deviate too much from that generated by SMOOTH; thereby remaining a smooth distribution.

The optimization procedure is illustrated in Figure 14 that consists of eight steps:

1. Compute steady background flow for ZTRAN using ZEUS steady aerodynamics analysis tool.

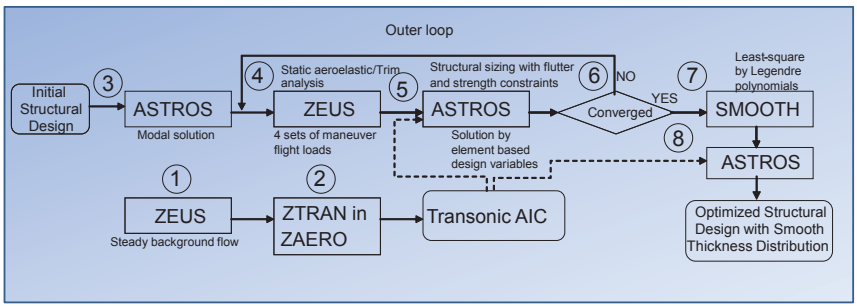

Figure 14: The flowchart of the aeroelastic tailoring.

2. With the computed steady background flow, the transonic AIC matrix is calculated using ZTRAN to be used in ASTROS for flutter constraint evaluation.

3. Execute ASTROS modal analysis for initial structural design, and provide modal solution for ZEUS.

4. Perform static aeroelastic/trim analysis using ZEUS at four flight conditions: 2.5g pull-up, -1.0g push-over, $\pm 25^\circ$ aileron deflection, with the design safety factor 1.5, generates the critical design loads.

5. Execute ASTROS sizing optimization to determine the design variables for a minimum weight design while satisfying the strength and flutter constraints.

6. If the result computed by Equation 5 is very small, the outer loop is converged. Otherwise, the modal solution of the optimized structure from this current outer loop is provided to ZEUS for the calculation of the new critical design loads. These new critical design loads are used for the subsequent ASTROS sizing optimization. This outer loop continues until the result computed Equation 5 is very small.

7. Apply the SMOOTH code to the thickness distribution computed by the final outer loop iteration to define the lower bound of each design variable for the final ASTROS optimization.

8. Perform the final ASTROS optimization to ensure that all constraints are satisfied and to obtain the final optimized structural design with smooth thickness distribution of all layers.

6 Results

6.1 Convergence History of ASTROS Optimization Process

Figure 15 presents the convergence history of the eight steps described in Section 5.4. Only 5 iterations are required to achieve a converged solution for the outer loop. After applying the SMOOTH code to the thickness distribution computed by the fifth outer loop iteration, the final ASTROS optimization gives the wing and truss weight of 1.363 tons for the optimized structure. Usually, the total wing spar, rib and skin weight of the same class of conventional aircraft like B737 is about one ton per wing. Therefore, the optimized wing and truss weight of the truss-braced wing is heavier than the conventional aircraft by 363kg for one wing or by 726kg for both wings. The total number of ASTROS iterations is 88, and total computational time is 45 hours.

6.2 Optimization Results Using ASTROS

Figure 16 and Figure 17 show the element thickness of the wing upper and lower skins for 0° and 45°,-45° and 90° laminates, respectively. It should be noted that for a better visual illustration, the element thickness shown in Figure 16 is actually 50 times of the realistic element thickness obtained from the optimization process. Three sets of thickness distribution are presented in each Figure which corresponds to the thickness

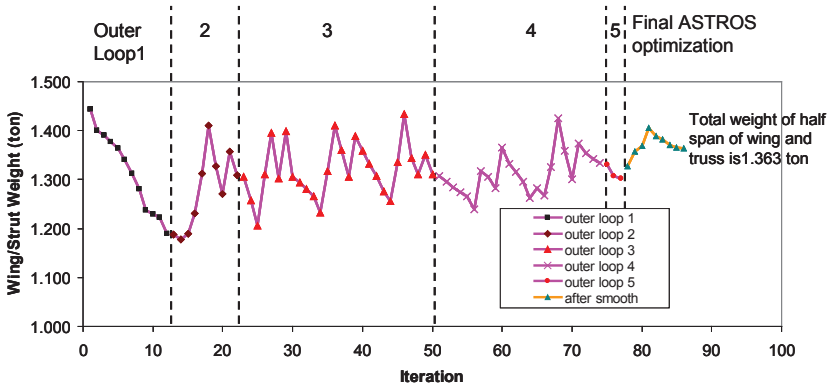

Figure 15: The convergence history of outer loop iteration in ASTROS optimization process.

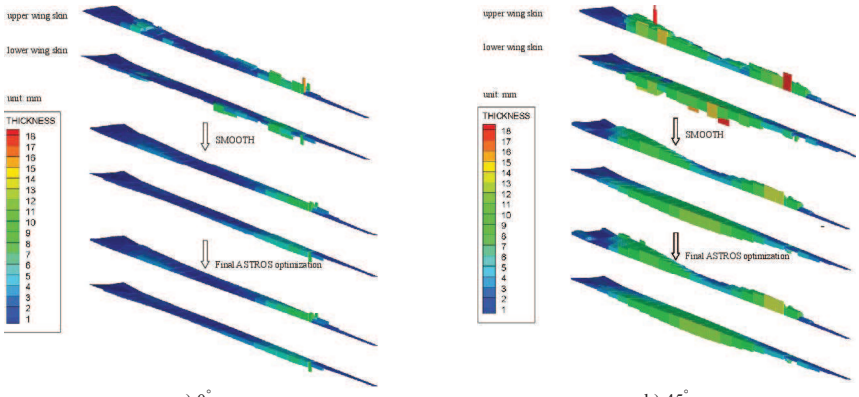

a) 0° b) 45°

Figure 16: The optimization results of the wing upper/lower skins at $0°$,$45°$ laminates.

distributions after the fifth outer loop iteration (top), after applying the SMOOTH code (middle) and computed by the final ASTROS optimization (bottom). It can be seen that spikes appear in the thickness distributions computed by the fifth outer loop iteration which leads to a non-smooth distribution. The SMOOTH code removes those spikes and adds thickness to those regions that have sudden reduction in thickness; rendering a smooth thickness distribution. The final ASTROS optimization adds small thickness to several elements for satisfying all strength and flutter constraints. Comparing to those computed by the fifth outer loop iteration, the thickness distributions of each composite layer computed by the final ASTROS optimization are much smoother. In other words, the final ASTROS optimization can achieve a smooth thickness distribution by paying a small weight penalty.

Finally, the thickness distributions of the four composite layers on the upper and lower skins of the wing and truss are presented by color maps in Figure 18 and Figure 19, respectively.

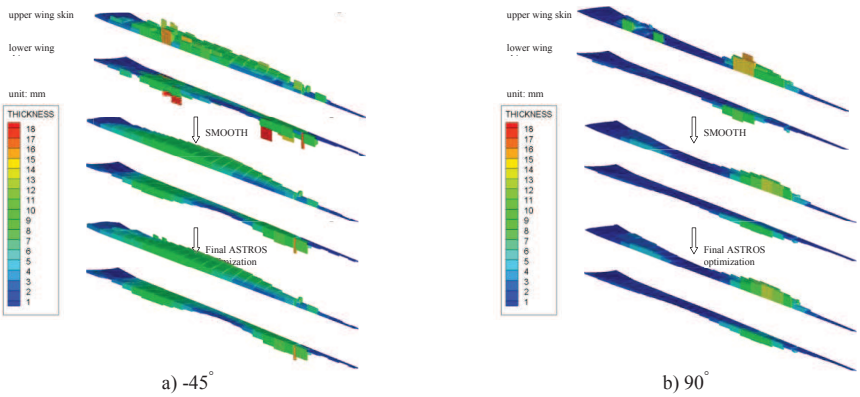

a) -45° b) 90°

Figure 17: The optimization results of the wing upper/lower skins at $-45°$,$90°$ laminates.

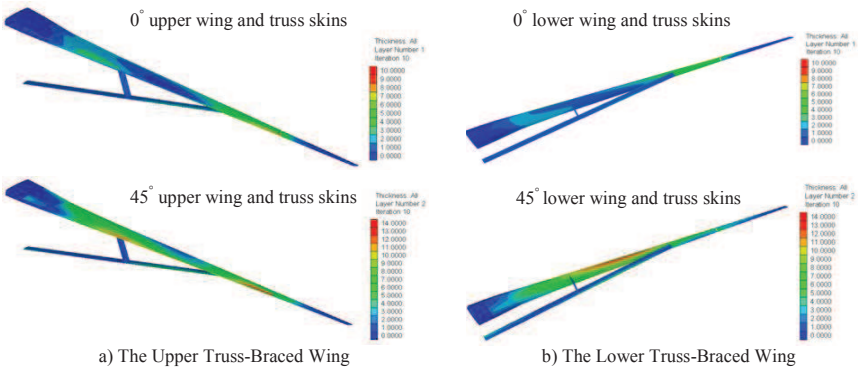

a) The Upper Truss-Braced Wing b) The Lower Truss-Braced Wing

Figure 18: The upper/lower wing and truss skin thickness at 0° ,45° laminates.

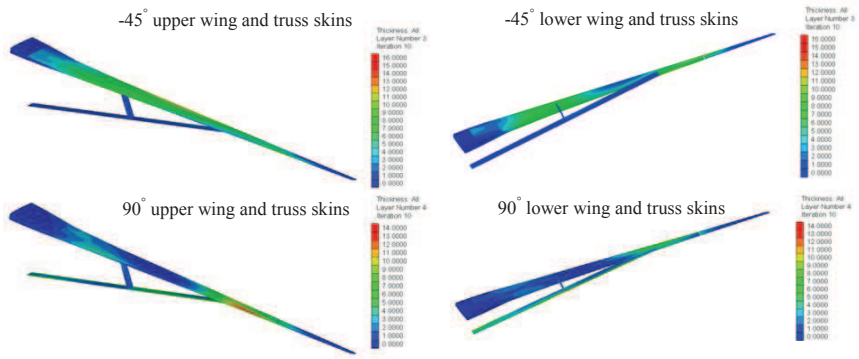

a) The Upper Truss-Braced Wing b) The Lower Truss-Braced Wing

Figure 19: The upper/lower wing and truss skin thickness at -45° ,90° laminates.

6.3 Strains and Deformations by the Final ASTROS Optimization

As described in previous section, at Mach number 0.72, four maneuvering flight conditions are screened to calculate the critical loads: 2.5g pull-up, -1.0g push-over, $\pm 25^\circ$ aileron deflections. The strains and deformations of the structure designed by the final ASTROS optimization at these four flight conditions are presented in Figure 20 and and Figure 21, respectively. Also, the un-deformed structure is shown in Figure 20 and Figure 21 by the blue color. It can be seen that all strains are between the strain constraints $[-0.004 \sim 0.006]$; verifying that all strength constraints are satisfied. In addition, the minimum strain -0.0040 and the maximum strain 0.0060 appear in those strains induced by the design loads at 2.5g pull-up condition and the minimum strain -0.00407 appears in those at the 25° aileron deflection condition; indicating that the strains induced by the loads at these two flight conditions dominate the structural design.

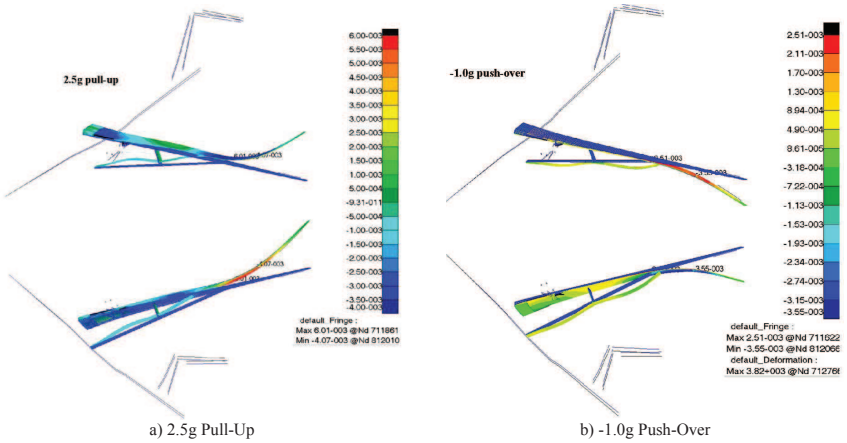

a) 2.5g Pull-Up b) -1.0g Push-Over

Figure 20: The strain and deformation of the wing structure at 2.5 pull-up (left) and -1.0g push-over (right).

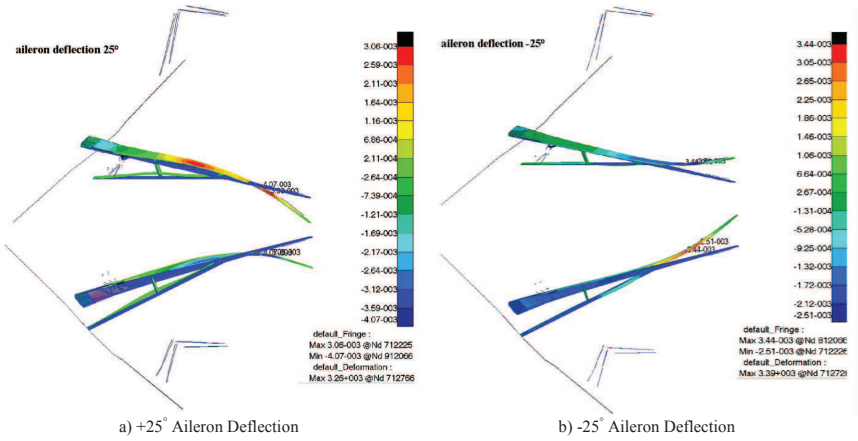

a) +25° Aileron Deflection b) -25° Aileron Deflection

Figure 21: The strain and deformation of the wing structure at $+25^\circ$ aileron deflection (left) and -25° aileron deflection (right).

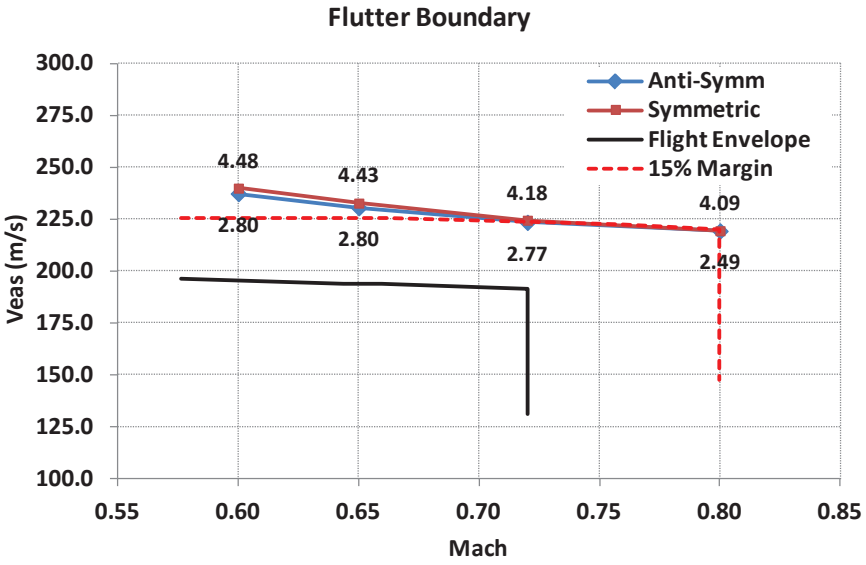

Figure 22: The flutter boundary after optimization process.

6.4 Flutter Boundary by the Final ASTROS Optimization

Figure 22 presents the symmetric flutter boundary (shown by the solid red line) and the anti-symmetric flutter boundary (shown by the solid blue line) along with their flutter frequencies of the structure designed by the final ASTROS optimization. The designed flight envelope in terms of equivalent air speed (Veas) versus Mach number is indicated using black line, and the 15% flutter margin requirement above the designed flight envelope is indicated using red dashed line. It can be seen that the flutter speeds at Mach numbers 0.72 and 0.8 barely satisfy the 15% flutter margin requirement; indicating that, in additional to the strength constraints, these flutter constraints also dominate the structural design.

7 Comparison to Aircraft with Conventional Configuration

In order to compare the flight performance of the truss-braced natural-laminar-flow wing aircraft with the conventional aircraft, the Breguet equation is applied to compute the range or fuel.

$$R = V \cdot \frac{C_L}{C_D} \cdot \frac{1}{c_f} \cdot ln(\frac{W_i}{Wf}) \tag{6}$$

where R is the range, V is the air speed, C_L is the lift coefficient, C_D is the drag coefficient, c_f is the fuel consumption rate, W_i is take-off weight of the aircraft, and W_f is the landing weight of the aircraft.

Table 4 compares the performance between the truss-braced wing aircraft designed by this research effort and a conventional civil aircraft similar to B737. From Table 4, it shows that the truss-braced wing aircraft has higher lift-to-drag ratio than that of the

	Aircraft (B737 size)	Truss-braced wing aircraft(30% transition)	Truss-braced wing aircraft(50% transition)
Weight(tons)	87.0	87.6	87.6
Cruise Mach	0.78	0.71	0.72
C_L/C_D	18	22.39	28.71
Range (with same fuel)	100%	112%	146%
Fuel (with same range)	100%	87%	65%

Table 4: Comparison of the truss-braced natural laminar wing aircraft with the conventional aircraft.

conventional civil aircraft. If the take-off weight of the conventional civil aircraft is 87 tons, then that of the truss-braced wing aircraft is 87.726 tons. Therefore, if both aircraft carry the same amount of fuel, according to the Breguet equation the truss-braced wing aircraft for the cases of assuming the laminar transition at 30% and 50% wing chord, respectively, has 12% and 46% longer range than the conventional civil aircraft. For the same range requirement, the truss-braced wing aircraft for the 30% and 50% laminar transition cases needs 13% and 35%, respectively, less fuel than the conventional aircraft. This comparison clearly shows the advantages of the truss-braced wing configuration over the conventional civil aircraft.

8 Conclusion

In this paper, an aeroelastic tailoring design study for a truss-braced natural-laminar-flow composite wing aircraft with high aspect ratio is investigated. Using composite material and applying aeroelastic tailoring technique by ASTROS, the optimized wing structure of the truss-braced wing aircraft can satisfy both strength and flutter constraints without paying a large weight penalty. The results show that comparing to the same class of commercial aircraft such as B737, the structural weight of the truss-braced wing aircraft increases only 726kg. However, the lift-to-drag ratio CL/CD can increase 24% (for the laminar flow transition point as 30% of chord length), or 60% (if transition points located at 50% of chord length) which can lead to 13% and 35% of fuel saving, respectively; this suggests that the truss-braced natural-laminar-flow composite wing configuration has the great potential in the future commercial aviation market.

References

[1] V.V. Chedrik, F.Z. Ishmuratov, S.I. Kuzmina, and M.C. Zichenkov. Strength/aeroelasticity research at mutidisciplinary structural design of high aspect ratio wing. In *27th International Congress of the Aeronautical Sciences*, 2010.

[2] W. Pfenninger. Laminar flow control laminarization. Technical report, 1976. AGARD Report 654.

[3] J.E. Green. Laminar flow control-back to the future. In *38th Fluid Dynamics Conference and Exhibit*, 2008. AIAA-2008-3738.

[4] W. Pfenninger. Design consideration of large subsonic long range transport airplanes with low drag boundary layer suction. Technical report, Northrop Aircraft, Inc, November 1954. Report NAI-54-800(BLC-67).

[5] C.E. Jobe, R.M. Kulfan, and J.D. Cachal. Wing planforms for large military transports. In *AIAA Atmospheric Flight Mechanics Conference and Exhibit*, 1978. AIAA-1978-1470.

[6] R.V. Turriziani, W.A. Lovell, G.L. Martin, J.E. Price, E.E. Swanson, and G.F. Washburn. Preliminary design characteristics of a subsonic business jet concept

employing an aspect ratio 25 strut-braced wing. Technical report, October 1980. NASA-CR-159361.

[7] P.M. Smith, J. De Young, W.A. Lovell, J.E. Price, and G.F. Washburn. A study of high-altitude manned research aircraft employing strut-braced wings of high-aspect-ratio. Technical report, February 1981. NASA-CR-159262.

[8] J.M. Grasmeyer. Multidisciplinary design optimization of a transonic strut-braced wing aircraft. In *37th AIAA Aerospace Sciences Meeting and Exhibit*, 1999. AIAA-1999-0010.

[9] IV J.F. Gundlach, P-A. Tbtrault, F. Gern, A. Nagshineh-Pour, A. Ko, J.A. Schetz, W.H. Mason, R. Kapania, and B. Grossman. Multidisciplinary design optimization of a strut-braced wing transonic transport. In *AIAA Aerospace Science Meeting and Exhibit*, 2000. AIAA-2000-0420.

[10] IV J.F. Gundlach, F.H. Tetrault, P.A.and Gern, A.H. Nagshineh-Pour, A. Ko, J.A. Scheta, W.H. Mason, R.K. Kapania, B. Grossman, and R.T. Haftka. Systematic review of the impact of emissions from aviation on current and future climate. *Journal of Aircraft*, 37(6):976–983, 2000.

[11] F.H. Gern, A. Ko, E. Sulaeman, R.K. Kapania, W.H. Masonm, and B. Grossman. Passive load alleviation in the design of a strut-braced wing transonic transport aircraft. In *AIAA/USAF/NASA/ISSMO Symposium and Multidisciplinary Analysis and Optimization*, 2000. AIAA-2000-4826.

[12] F.H. Gern, A.H. Naghshineh-Pour, E. Sulaeman, R.K. Kapania, and R.T. Haftka. Structural wing sizing for multidisciplinary design optimization of a strut-braced wing. *Journal of Aircraft*, 38(1):154–163, 2001.

[13] F. Gern, A. Ko, and R. Haftka. Transport weight reduction through mdo: The strut-braced wing transonic transport. In *35th AIAA Fluid Dynamics Conference and Exhibit*, 2005. AIAA-2005-4667.

[14] O. Gur, M. Bhatia, J.A. Schetz, W.H. Mason, R.K. Kapania, and D.N. Mavris. Design optimization of a truss-braced wing aircraft. In *9th AIAA Aviation Technology, Integration, and Operations Conference*, 2009. AIAA-2009-7114.

[15] M. Bhatia, R.K. Kapaniay, M. van Hoekz, and R.T. Haftka. Structural design of a truss braced wing: Potential and challenges. In *50th AIAA/ASME/ASCE/AHS/ASC Structures, Structural Dynamics, and Materials Conference and Exhibit*, 2009. AIAA-2009-2147.

[16] M. Bhatia, R.K. Kapaniay, O. Gurz, J.A. Schetzx, W.H. Mason, and R.T. Haftka. Progress towards multidisciplinary design optimization of truss braced wing aircraft with flutter constraints. In *13th AIAA/ISSMO Multidisciplinary Analysis Optimization Conference*, 2010. AIAA-2010-9077.

[17] O. Gur, M. Bhatia, J.A. Mason, W.H. Schetz, , R.K. Kapania, and T. Nam. Development of framework for truss-braced wing conceptual MDO. In *51st AIAA/ASME/ASCE/AHS/ASC Structures, Structural Dynamics, and Materials Conference*, 2010. AIAA-2010-2754.

[18] O. Gur, M. Bhatia, J.A. Schetz, W.H. Mason, R.K. Kapania, and D.H. Mavris. Design optimization of a truss-braced-wing transonic transport aircraft. *Journal of Aircraft*, 47(6):1907–1917, 2010.

[19] D. Alexander, Y.M. Lee, M. Guynn, and D. Bushnell. Emissionless aircraft study. In *38th AIAA/ASME/SAE/ASEE Joint Propulsion Conference and Exhibit*, 2002. AIAA-2002-4056.

[20] K. Takeda, A.L. Tekada, J. Bryant, and A.J. Clegg. Systematic review of the impact of emissions from aviation on current and future climate. *The Aeronautical Journal*, 112(1135):493–522, 2008.

[21] M.K. Bradley and C.K. Droney. Subsonic ultra green aircraft research: Phase i final report. Technical report, 2011. NASA/CR-2011-216847.

[22] M.K. Bradley and C.K. Droney. Subsonic ultra green aircraft research phase ii: N+4 advanced concept development. Technical report, 2012. NASA/CR-2012-217556.

[23] M.H. Shrik, T.J. Hertz, and T.A. Weisshaar. Aeroelastic tailoring- theory, practice, and promise. *Journal of Aircraft*, 23(1):6–18, 1986.

[24] Y. Harmin and J. Cooper. Aeroelastic tailoring using ant colony optimization. In *50th AIAA/ASME/ASCE/AHS/ASC Structures, Structural Dynamics, and Material Conference and Exhibit*, 2009. AIAA-2009-2194.

[25] P.C. Chen. *ASTROS Theoretical Manual*. ZONA Technology Inc, Scottsdale, Version 21.2 edition, February 2012.

[26] P.C. Chen. *ZAERO Theoretical Manual*. ZONA Technology Inc, Scottsdale, Version 8.1 edition, July 2007.

[27] P.C. Chen. *ZEUS Theoretical Manual*. ZONA Technology Inc, Scottsdale, Version 3.2 edition, February 2012.

[28] Q. Li. The fuselage structural mass distribution analysis of a commercial aircraft. Technical report, COMAC, February 2012.

[29] Q. Li. The t-tail structural mass distribution analysis of a commercial aircraft. Technical report, COMAC, February 2012.

[30] M. Spick. *McDonnell Douglas F/A-18 Hornet*. Salamander Books, London, 1991.

[31] J.H. Zhao. The whole aircraft mass distribution analysis of a commercial aircraft. Technical report, COMAC, August 2012.

[32] P.C. Chen, X.W. Gao, and L. Tang. Overset field-panel method for unsteady transonic aerodynamic influence coefficient matrix generation. *AIAA Journal*, 42(9):1775–1787, 2004.